Magnetism of iron on tungsten (001) studied by spin-resolved scanning tunneling microscopy and spectroscopy

K. von Bergmann,* M. Bode, and R. Wiesendanger
Institute of Applied Physics and Microstructure Research Center, University of Hamburg, Jungiusstrasse 11, 20355 Hamburg, Germany
(Received 18 December 2003; revised manuscript received 1 July 2004; published 30 November 2004)

The system of Fe on W(001) has been investigated using spin-integrated as well as spin polarized scanning tunneling microscopy and spectroscopy. The electronic structure in the pseudomorphic growth regime and the beginning of strain relief has been studied and a pronounced layer dependence of the differential conductance has been observed. The spin-resolved measurements focus on the magnetic structure in the pseudomorphic regime. The domain structure is investigated with high spatial resolution and the fourfold anisotropy can directly be deduced from the maps of differential conductance. Quantitative analysis of the intensity of the signal reveals a layer dependent easy axis in the pseudomorphic regime. While the second and third monolayer are magnetized along ⟨110⟩ directions of the surface the fourth monolayer has an easy axis along ⟨100⟩. These high-symmetry directions and therefore also the layer-dependent easy axes enclose an angle of 45°.

DOI: 10.1103/PhysRevB.70.174455 PACS number(s): 75.70.Rf, 68.37.Ef, 75.30.Gw

I. INTRODUCTION

Magnetism of reduced dimensions is a fascinating topic which still holds a lot of barely understood phenomena.[1] For the understanding of magnetic properties in general it is indispensable to study the basic properties in nanometer-scale systems where changes in structure or size have large effects on the magnetic properties. Model systems for magnetism of reduced dimensions are magnetic thin films or islands on nonmagnetic substrates. A wide variety of thin-film systems have shown a thickness dependent change in anisotropy.[2–8] Also size dependent effects have been studied and it has been observed that different magnetic ground states are realized connected with the morphology of the system.[9–11]

There has been a lot of interest in the magnetic properties of highly strained pseudomorphic Fe films on W(001). The structural properties have been studied by various spatially averaging[12–14] and high-resolution methods.[15,16] It was consistently found that independent of the growth temperature ($T \geqslant 300$ K) the first monolayer initially wets the W(001) substrate. This Fe wetting layer is thermodynamically stable up to the desorption temperature ($T \approx 1200$ K). In contrast, the growth mode of the following Fe layers critically depends on the substrate temperature and/or annealing conditions. At room temperature the atom mobility is rather low leading to relatively rough films that consist of small islands with a typical diameter of about 10 nm and a blurred low-energy electron-diffraction (LEED) pattern.[15] The film quality can be improved by moderate annealing at $400\ \text{K} \leqslant T \leqslant 600$ K as indicated by a sharp LEED pattern and larger islands. Only at annealing/growth temperatures $T \geqslant 600$ K the Fe films break up into relaxed three-dimensional islands on top of a closed pseudomorphic 2 monolayer (ML) carpet.[15]

Contrary results have been reported concerning the magnetic properties of Fe films on W(001) in the low coverage regime which have mainly been studied by spatially averaging methods.[13–22] At coverage $\theta \leqslant 1$ ML no magnetic signal was found which was attributed to a paramagnetic or antiferromagnetic state.[20] *Ab initio* density-functional theory calculations supported the latter explanation.[23] According to early magneto-optical Kerr effect (MOKE) measurements[17] the easy magnetization axis of 1–3 ML Fe/W(110) is along ⟨110⟩ directions.[18,19] In contrast, the results of spin polarized electron-diffraction experiments were interpreted in terms of a ⟨100⟩ easy axis.[13,21] Recent MOKE data, however, confirm the former measurements, i.e., that the easy axis of room-temperature grown films is along the ⟨110⟩ axis up to a coverage $\theta \approx 6$ ML.[15,16] Only for higher coverage a ⟨100⟩ easy axis is observed. Growth at a substrate temperature $T = 400$ K shifts this spin reorientation transition to the slightly lower coverage of the onset of dislocation formation (local coverage $\theta \geqslant 5$ ML).[15,16]

Since it is well known that different morphologies can lead to diverse magnetic structures the importance of investigating the structure as well as the magnetic properties with high spatial resolution to fully understand a system is obvious. Spin polarized scanning tunneling microscopy (SP-STM) satisfies the criteria mentioned and thus is a powerful tool to study the magnetism of reduced dimensions and correlate it directly to the topographic as well as the electronic structure.[24,25] To overcome the discrepancy concerning the magnetic properties of thin Fe films on W(001) we used SP-STM to investigate the system: this method is magnetically sensitive and has a high spatial resolution which allows not only the investigation of magnetic properties but also a direct correlation to electronic structure measurements and detailed topographic studies.

This paper is organized as follows: After a brief introduction into the experimental setup and the measurement procedures (Sec. II) we will discuss the results obtained on reconstructed islands with a local coverage just above the onset of relaxation (Sec. III A) and on pseudomorphic films (Sec. III B). In both cases structural and spin-averaged electronic properties are directly correlated. Additionally, spin-resolved data measured on pseudomorphic films (Sec. III B) reveal a nanometer-scale local coverage dependent rotation of the easy axis. While the second and third monolayer are magne-

tized along ⟨110⟩ directions, fourth monolayer patches have an easy axis along ⟨100⟩. The results will be summarized in Sec. IV.

II. EXPERIMENT

The experiments have been performed in an ultrahigh vacuum (UHV) system consisting of separate chambers for preparation, molecular-beam epitaxy, standard surface science analysis methods such as low-energy diffraction (LEED) and Auger electron spectroscopy, and a chamber holding a cryogenic STM.[26] The base pressure in all chambers is in the low 10^{-9}Pa regime. The W(001) substrate is cleaned by cycles of annealing ($T \approx 1700$ K) in oxygen atmosphere ($p_{O_2} \approx 5 \times 10^{-5}$Pa) for 20 min and a subsequent short flash to high temperature ($T \approx 2500$ K) in UHV.[16] Fe is evaporated from a rod heated by electron bombardment at a rate of ≈1 ML per minute with $p \leqslant 1 \times 10^{-8}$ Pa. The coverage θ is always given in pseudomorphic monolayers and in the context of spatially resolved measurements refers to the local coverage. The growth mode of Fe on the W(001) substrate can be influenced by simultaneous or subsequent heating of the sample which is done by indirect heating. The temperature is measured via a thermocouple attached to the manipulator in close vicinity to the sample. After preparation the sample is transferred to the cryogenic STM which also holds a tip exchange mechanism. Spin-integrated measurements are preformed with W tips chemically etched from a polycrystalline wire. For spin-resolved measurements these tips are flashed *in vacuo* to remove any contaminants. Coating with ≈10 ML of Fe and subsequent moderate annealing leads to a magnetic in-plane sensitivity referring to the sample surface.[24,25] During measurements tip and sample are held at $T = 13 \pm 1$ K. All topographic images are measured in constant current mode. Differential conductance (dI/dU) signals are obtained using lock-in technique with a modulation voltage $U_{mod} \approx 10-20$ mV of frequency $f \approx 3-8$ kHz added to the bias voltage. While dI/dU spectra are acquired with an open feedback loop at the given stabilization parameters, dI/dU maps are measured with closed loop at the indicated voltage.

III. RESULTS AND DISCUSSION

In the following the growth modes of Fe on W(001) in the low coverage regime are studied. Topographic images are correlated with electronic structure measurements and the magnetic properties in the pseudomorphic growth regime are investigated.

A. Transition from pseudomorphic growth to strain relief

Preparation of a sample of Fe on W(001) with moderate annealing of the substrate during evaporation of Fe leads to a morphology with different local coverage in the regime of a few monolayers. For $\theta \geqslant 2$ ML a pseudomorphic wetting layer of 2ML is always observed. The 3rd and 4th ML also grow pseudomorphically but not in a strict layer-by-layer growth mode. Beginning with the 5th ML strain is relieved by incorporation of dislocation lines along ⟨100⟩. They form a regular pattern which was identified to be a (9×1) superstructure.[15]

1. Topography

Figure 1(a) shows the topography of 5.1 ML of Fe evaporated onto the sample held at $T \approx 550$ K. The elongated islands along the ⟨100⟩ directions of the surface are of local coverage ⩾5 ML. As we will show below they exhibit dislocation lines along the long axis of the islands. While the topography image of Fig. 1(a) only allows the discrimination between reconstructed and pseudomorphic areas, the dI/dU map at $U = +0.2$ V shown in Fig. 1(b) makes it possible to distinguish between different local coverages. Besides the fact that at this voltage the dI/dU signal is generally larger on reconstructed islands compared to the signal on pseudomorphic areas, three different contrasts can be identified in the latter case. This leads to the conclusion that different dI/dU signals correspond to different local coverages, in this case to the 2nd, 3rd, and 4th ML. Closed areas which show two different contrasts are constituted of areas with two different local coverages and a tungsten step underneath the surface. The positions of these buried substrate step edges are indicated with letters a–e in Fig. 1(b). The information gained from the topographic image together with the dI/dU map leads to an assignment of local coverage as demonstrated for the line profiles in Fig. 1(c) and 1(d). The plots are taken at the position of the lines in (a) and (b), respectively. The three different dI/dU contrasts in the pseudomorphic growth regime can be identified as follows: the darkest one corresponds to a local coverage of 2 ML, the medium one to 3 ML while the brightest contrast can be assigned to 4 ML. The local coverage along the height profile is schematically illustrated in Fig. 1(c). The sample surface is composed of ≈10% of 2nd ML, ≈15% of 3rd ML, ≈25% of 4th ML, and ≈40% of $\theta \geqslant 5$ ML.

After identification of the different pseudomorphic coverage regimes the apparent height of the layers is investigated. Figure 2(a) shows a closer view of the topography at the section of the surface indicated by the dashed rectangle in Fig. 1(a). The dashed line marks a buried monoatomic step of the tungsten substrate from an upper terrace (left) to a lower terrace (right). Again one can easily discriminate unequal local coverage due to different electronic structure of the layers in the dI/dU map at $U = +0.9$ V in Fig. 2(b). The local coverage is indicated in Fig. 2(a) with 2, 3, and 4 ML for the pseudomorphic regime and A, B, and C for the reconstructed areas. Figure 2(c) displays a model of the (9×1) reconstruction which is formed for $\theta \geqslant 5$ ML assuming that one additional atom is incorporated per dislocation line. The histograms of Fig. 2(d) show the measured height distribution on the two terraces of the W substrate of Fig. 2(a). The darker line is a histogram of the left terrace, with the dominating local coverage of 2 ML, 3 ML, and coverage denominated with C. The brighter line in Fig. 2(d) corresponds to the right tungsten terrace of Fig. 2(a) with a local coverage of 4 ML, A, B, and C. In order to compensate the height of the monoatomic step of the tungsten substrate the height axes of the two lines are shifted by 1.6 Å with respect

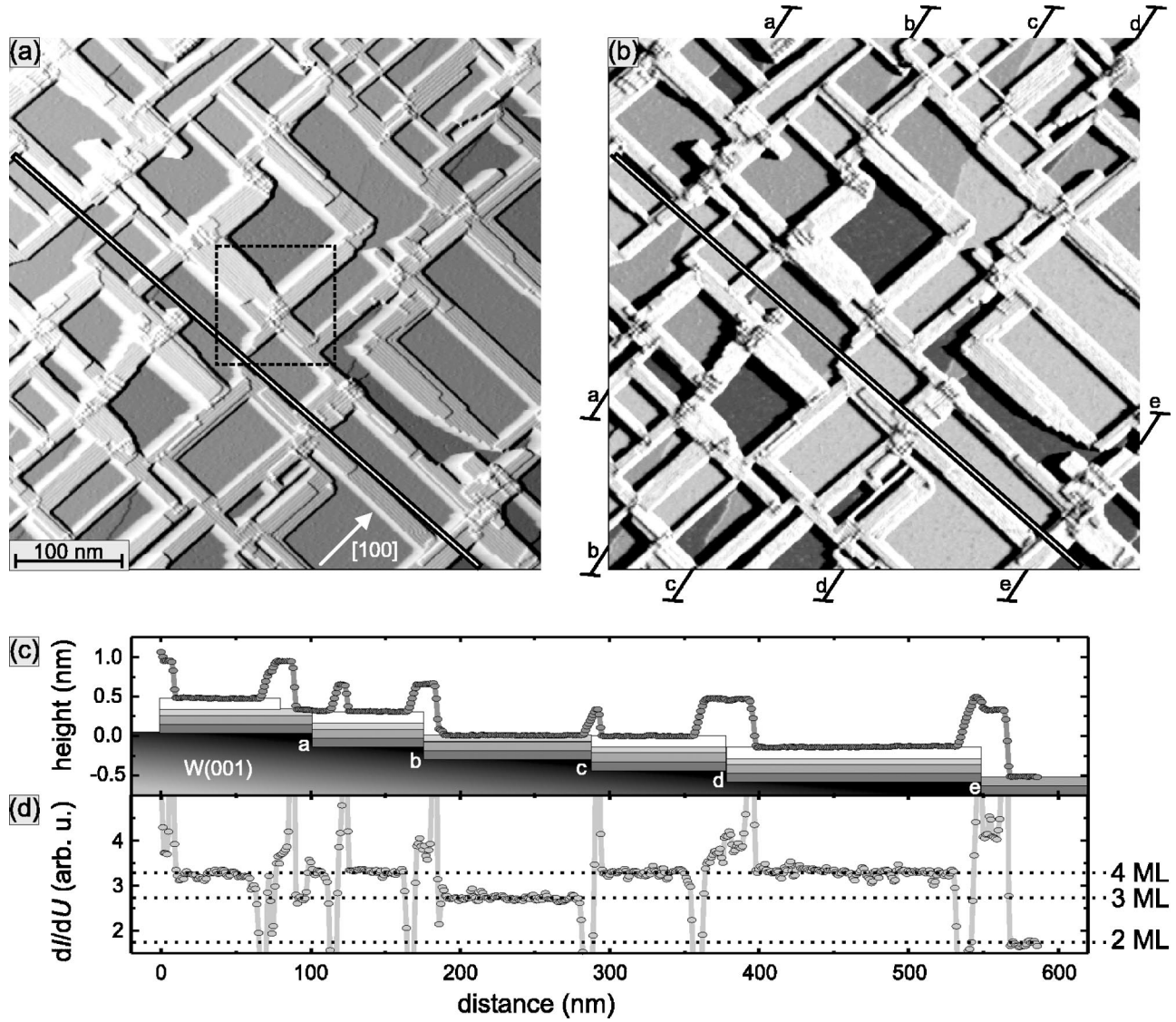

FIG. 1. Sample of 5.1 ML of Fe on W(001) grown at $T \approx 550$ K. (a) Topography, the dashed rectangle marks the image area investigated more closely in Fig. 2; (b) dI/dU map corresponding to (a) at $U=+0.2$ V, the marks (a–e) indicate steps of the underlying W(001) substrate; (c) height profile along the line in (a) with a sketch of the local coverage; (d) corresponding dI/dU signal along the line in (b) with dotted lines indicating the signal strength for the different local coverage.

to each other. We observe sharp peaks which are assigned to a local coverage of 2, 3, and 4 ML and broader ones for coverage labeled A, B, and C with the splitting due to protrusions and depressions of the reconstruction. The height difference between adjacent peaks is given in Å. The bulk lattice constant for bcc W is $a_W=3.165$ Å and for Fe it is $a_{Fe}=2.8665$ Å.[27] Considering a bcc (001) surface one expects an ideal monoatomic step for W to be $h_W=1.583$ Å and for Fe $h_{Fe}=1.433$ Å. We observe a large variation of the apparent height in the low coverage regime which suggests different electronic properties of the layers. The large height difference of $h=3.01$ Å between the 4th ML and layer A could correspond to one additional layer, two layers, or even three monolayers with a height of $h=1$ Å each.

In order to evaluate which assumption is the most probable we want to discuss the consequence of the formation of the reconstruction and the height of reconstructed areas. There are different approaches to approximate the influence of strain on the dimensions of materials. For bulk materials the Poisson ratio ν is a measure for variations in length due to compression or elongation in the perpendicular direction (with $\nu_{Fe}=0.29$).[27] Total-energy calculations for the system of 2 ML Fe/W(001) predict an interlayer distance between the two pseudomorphic iron layers of 1.09 Å which can be understood on the basis of a model with a constant atomic volume for metal atoms.[23] The height of uniaxial of biaxial strained layers derived from this simple model is about the same as an estimation with a Poisson ratio close to 1. This discrepancy in Poisson values results in a much larger inward relaxation of the pseudomorphic iron layers in the case of the model with constant atomic volume in contrast to an estimate with the bulk Poisson ratio. Experimental evidence of a large inward relaxation of the bilayer of Fe/W(001) has been found with spin-polarized low-energy-electron diffrac-

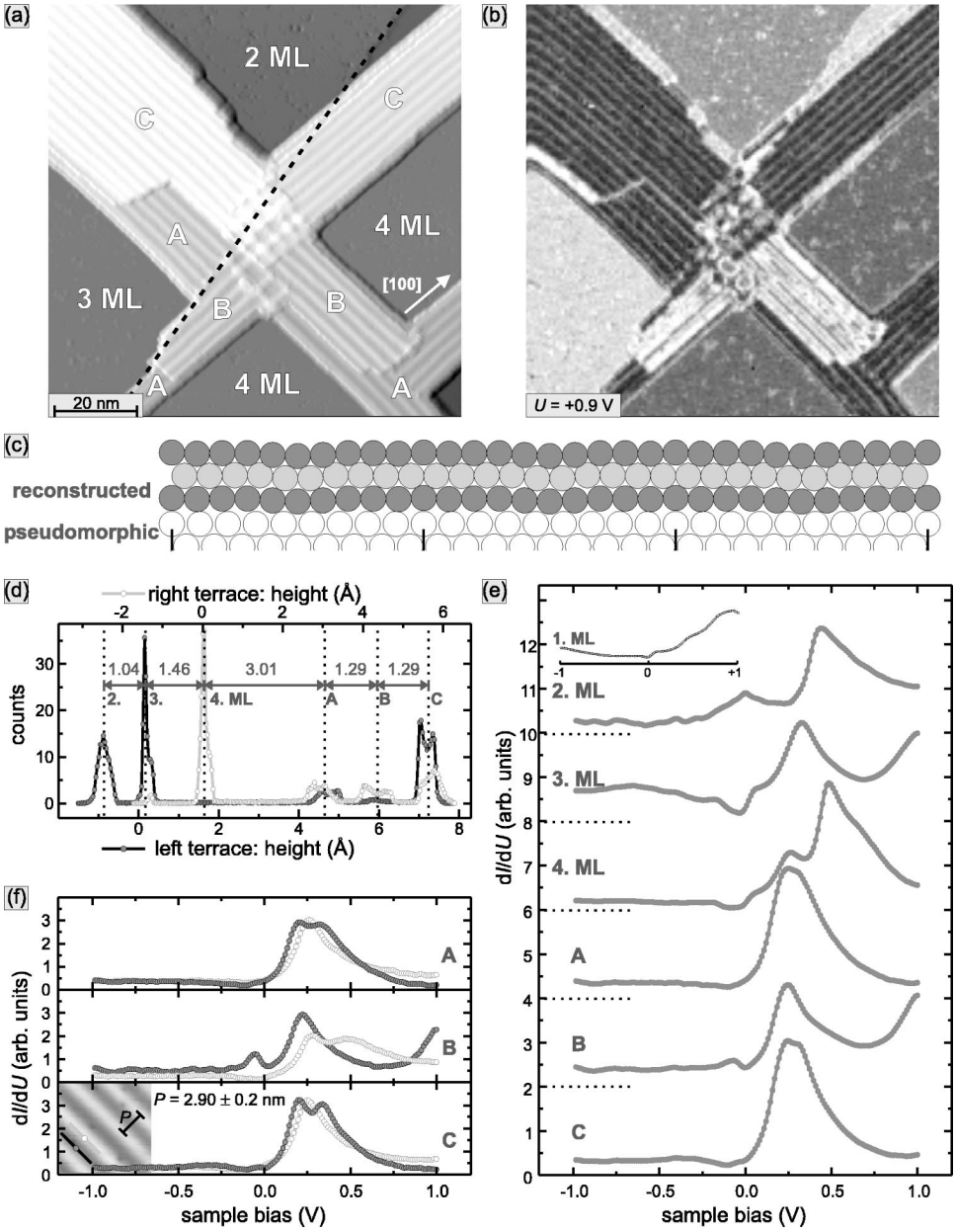

FIG. 2. Sample of 5.1 ML of Fe on W(001) grown at $T \approx 500$ K. (a) Topography at $U = +1.0$ V, the dashed line indicates a step of the tungsten substrate, labels refer to local coverage; (b) dI/dU map corresponding to (a) at $U = +0.9$ V taken from full spectroscopy (stabilization parameters: $U = +1.0$ V, $I = 1.0$ nA); (c) model of the (9×1) reconstruction cut along the [100] direction perpendicular to the dislocation lines; (d) histogram of left/upper and right/lower terrace in (a) shifted by 1.6 Å with respect to each other; (e) layer-resolved dI/dU spectra shifted by $dI/dU = 2$ arb. units for clarity, labels refer to the local coverage [cf. (a)]; inset, dI/dU spectrum of the 1st ML from a different measurement; (f) dI/dU spectra taken on protrusions and depressions of the reconstructed areas; inset, topography of local coverage indicated with C.

tion (SPLEED) and an interlayer distance between the two pseudomorphic iron layers of 1.20 Å was determined.[22] Comparing the results of the two models with the results from the total-energy calculation and the experimental SPLEED data we conclude that for the highly strained Fe films on W(001) with a lattice mismatch close to 10% the Poisson ratio for the bulk material is not valid anymore while a constant volume approach gives a good estimate of the interlayer distance.

Now the height derived from the STM measurements presented in this work is analyzed and compared to results obtained from this simple model assuming that the volume per atom does not change from fully relaxed to strained structures. With the bulk lattice constant of $a_{\mathrm{Fe}} = 2.8665$ Å for the unit cell with two atoms, the volume per Fe atom is $V_{\mathrm{Fe\text{-}atom}} = 11.777$ Å^3. In the pseudomorphic regime of Fe on tungsten (001) the area per atom is $A_{\mathrm{ps}} = 10.017$ Å^2. This leads to a height of $h_{\mathrm{ps}} = 1.176$ Å when the volume per atom is constant. In the reconstructed areas the strain is relieved in one $\langle 100 \rangle$ direction. The area per atom then is $A_{\mathrm{rc}} = 3.165$ Å $\times 2.849$ Å $= 9.017$ Å^2 which results in a height of $h_{\mathrm{rc}} = 1.306$ Å. The height of the 3rd and 4th ML as well as that of layers B and C are in reasonable agreement with this model. The height of four pseudomorphic monolayers of Fe on tungsten (001) in this simple model is $4 \times h_{\mathrm{ps}} = 4.704$ Å. Considering the measured value of 3.01 Å between 4th ML and layer A we calculate the height of layer A referred to the tungsten surface to be $h_{\mathrm{A}} = 7.714$ Å. It is assumed that layers which are pseudomorphic in the low coverage regime also relax and form the reconstruction to some extent once they are covered with patches of $\theta \geqslant 5$ ML.[16] In our simple model the height of layer A can be reproduced best when A is the 6th ML. Assuming one pseudomorphic layer and five reconstructed layers we calculate a height of $h_{\mathrm{A}} = 1 \times h_{\mathrm{ps}} + 5 \times h_{\mathrm{rc}} = 7.706$ Å. Even though we do not observe an intermediate height we conclude that layer A is the 6th ML and B and C

one additional layer each. We are, however, not able to directly prove this with the technique of STM. Therefore, we will keep the denominations A, B, and C.

2. Electronic structure

To investigate the electronic structure of the different local coverage regimes in more detail spatially resolved full dI/dU spectroscopy measurements were done in the sample area shown in Figs. 2(a) and 2(b). Figure 2(e) shows layer-resolved dI/dU spectroscopy data measured with stabilization parameters $U=+1.0$ V and $I=1.0$ nA. Even though each layer has a dominating spectral feature in the unoccupied states of the sample and is rather featureless in the occupied states, the fine structure of the layers proves to be quite layer dependent. The major peak for the pseudomorphic layers is observed at significantly different energies:

$$\text{at } U = +0.44 \text{ V for 2 ML},$$

$$\text{at } U = +0.33 \text{ V for 3 ML},$$

$$\text{at } U = +0.49 \text{ V for 4 ML}.$$

Theoretical calculations are necessary to reveal the cause and nature of the features in the dI/dU spectra.

The spectra of the reconstructed layers A and C show basically one peak and are very similar. Surprisingly the layer in between, labeled as B differs significantly. This becomes even more clear in Fig. 2(f) where the spectra are resolved to show the electronic structure on the protrusions and in the depressions of reconstructed areas. The period of the reconstruction is $P=2.9\pm0.2$ nm. Both region A and C show one peak in the dI/dU spectra at $U=+0.26$ V and +0.25 V, respectively, on the protrusions of the reconstruction and two peaks at $U\approx+0.20$ V and $U\approx+0.34$ V for the depressions. Region B shows quite different spectral features with one major peak at $U=+0.28$ V and a second one at $U=+0.50$ V on the protrusions. In the depressions one dominating peak in the unoccupied states at $U=+0.22$ V and an additional peak in the occupied states at $U=-0.05$ V of the sample is observed.

For a more detailed understanding of the impact of the reconstruction on the electronic structure theoretical calculations are necessary. The magnetic properties of samples similar to the one shown in Fig. 2 have been investigated previously with MOKE measurements.[15] It is proposed that they exhibit a fourfold anisotropy with easy directions along $\langle 110\rangle$ up to the onset of dislocation formation.

B. Pseudomorphic regime

The system of Fe on W(001) shows pseudomorphic growth when the local coverage is $\leqslant 4$ ML. Again the temperature of the substrate during evaporation determines the growth mode. The magnetic properties in the pseudomorphic regime have been studied with various techniques. No magnetization was found in the monolayer[14,15,22] but calculations predicted an antiferromagnetic ground state.[28] There have been contrary statements about the easy axis of the magnetization for the pseudomorphic layers. Surface magneto-optical Kerr effect measurements showed an easy axis along $\langle 110\rangle$ for 1.5 ML of Fe on W(001) (Ref. 19) but measurements with SPLEED of up to 5 ML were interpreted in terms of an easy axis along $\langle 100\rangle$ even though it was pointed out that a magnetic easy axis along $\langle 110\rangle$ is also possible.[13] Referring to the SPLEED measurements it was then assumed that the magnetization is along $\langle 100\rangle$ (Refs. 14 and 22) until MOKE measurements suggested an easy direction along $\langle 110\rangle$ for moderately annealed pseudomorphic films up to the onset of dislocation formation.[15] Using the method of SP-STM we investigated the magnetism in the pseudomorphic regime of Fe on W(001) with high spatial resolution.

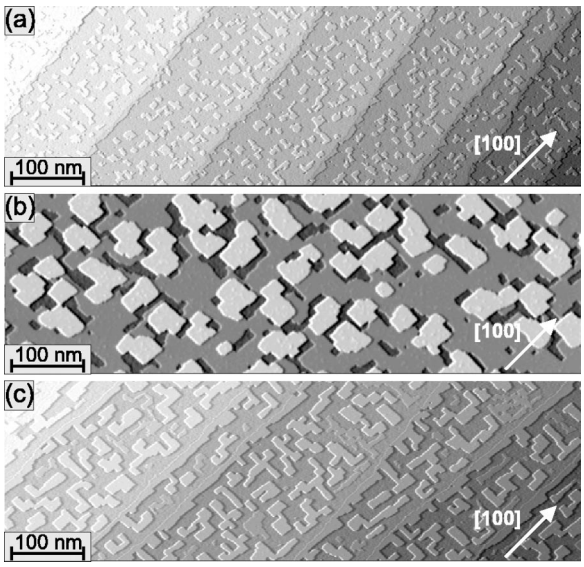

FIG. 3. Topography of Fe on W(001) in the pseudomorphic regime with different growth conditions. (a) 2.2 ML Fe on W(001) grown at $T\approx 525$ K; (b) 3.2 ML Fe on W(001) grown at $T\approx 525$ K; (c) 3.0 ML Fe on W(001) grown at $T\approx 550$ K.

Since the azimuth of in-plane sensitive magnetic tips is usually unknown, SP-STM measurements only hold information about *variations* of the sample magnetization with respect to the tip magnetization but are unable to determine the *absolute* direction of magnetization. The tunneling current between two spin-polarized electrodes I_{SP} can be described by

$$I_{SP}(\vec{r},U_0) = I_0[1 + P_s P_t \cos(\vec{M}_s,\vec{M}_t)], \tag{1}$$

where I_0 is the non-spin-polarized current. The indices stand for the sample (s) and the tip (t). P is the spin polarization and $\vec{M}$ the magnetization. Since I_0, P_s, P_t, and $\vec{M}_t$ are constant at a given voltage U for a specific layer, a variation in I_{SP} and therefore also dI/dU can be attributed to different directions of the sample magnetization $\vec{M}_s$ with respect to $\vec{M}_t$.

1. Topography

Figure 3 shows the topography of samples with different growth conditions. In all cases the W(001) is covered with a

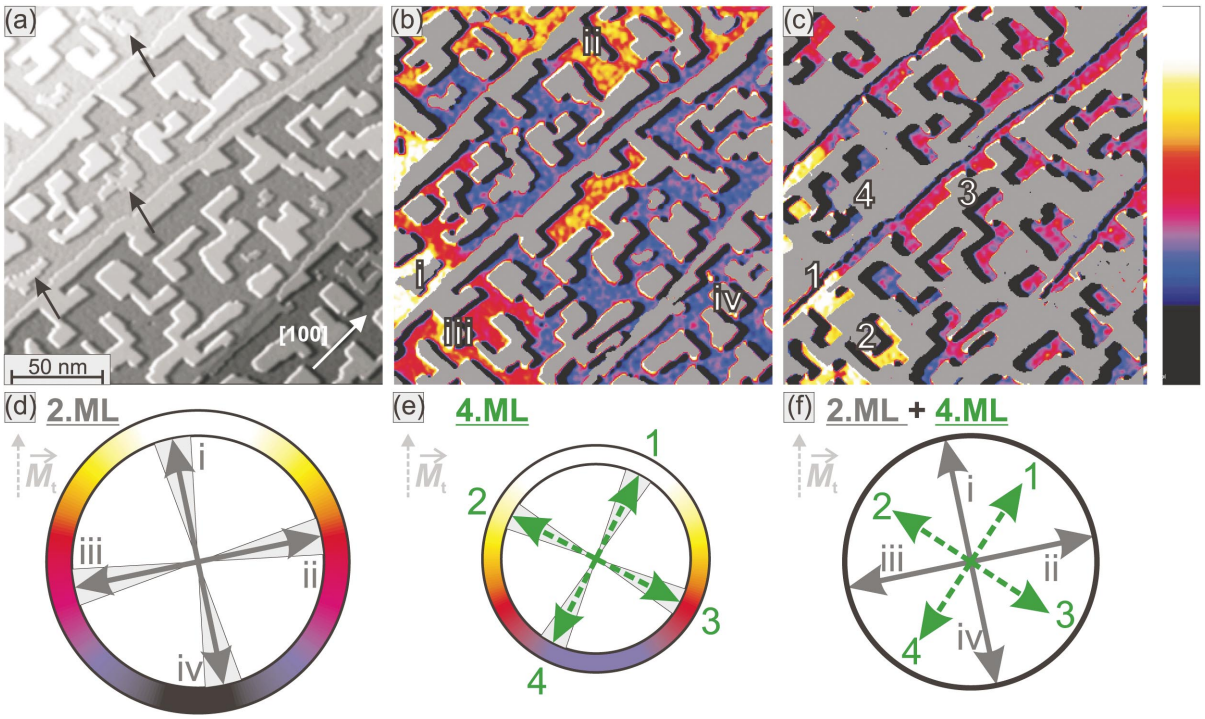

FIG. 4. (Color) Sample of 3.0 ML of Fe on W(001) grown at $T \approx 550$ K. (a) Topography, arrows indicate 3rd ML islands which will be referred to in Sec. III B 3; (b) corresponding dI/dU map measured at $U=-0.8$ V, color: 2nd ML /gray: 3, 4 ML; (c) dI/dU map corresponding to (a) at $U=-0.1$ V, color: 4th ML /gray: 2, 3 ML; (d) magnetization of 2nd ML with respect to tip magnetization; (e) magnetization of 4th ML with respect to tip magnetization; (f) sketch of the 45° rotation between 2nd and 4th ML magnetization.

2 ML thick wetting layer. When evaporating more than $\theta = 2$ ML of Fe onto a sample held at moderate temperature ($T \approx 525$ K) islands of the 3rd ML start to nucleate as shown in Fig. 3(a). When increasing the coverage islands of the 3rd ML grow and coalesce, but the 3rd ML remains uncompleted. As can be seen in Fig. 3(b) 4th ML islands start to form before the layer underneath is closed. Just as for small islands of the 3rd ML (a), the edges of the larger patches are preferably oriented along the ⟨100⟩ directions (b). The 4th ML islands on top are of a compact shape and also form edges along ⟨100⟩. At this temperature the interlayer mass transport is hindered and the proportions of the different layers can be quantitatively understood considering that once patches of the 3rd ML have been formed additional Fe is distributed onto 2nd and 3rd ML according to the percentage of the respective area. When increasing the temperature of the W(001) substrate during evaporation only slightly ($T \approx 550$ K) the growth mode changes dramatically as shown in Fig. 3(c). Only very few areas with a local coverage of 3ML are observed and they are of irregular shape. Islands of the 4th ML again have edges preferably oriented along the ⟨100⟩ directions but are of elongated shape, in contrast to the compact islands observed before (b). Obviously, the 3rd ML is thermodynamically unstable. When the temperature of the substrate is increased during growth, the mobility of the atoms is high enough to allow interlayer mass transport and a thermodynamically more stable sample is formed, consisting mainly of local coverage of 2 and 4 ML. The elongated shape of the 4th ML islands can be explained by a partial strain relief in the direction of the narrow axis of the island,

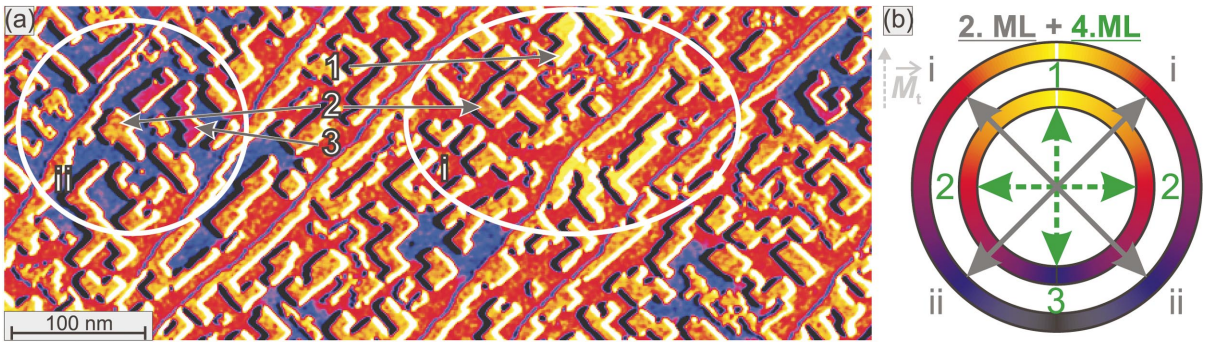

FIG. 5. (Color) Sample of 3.0 ML of Fe on W(001) grown at $T \approx 550$ K. (a) dI/dU map at $U=-0.1$ V; (b) sketch of the 45° rotation between 2nd and 4th ML magnetization.

which is only energetically favorable until a maximum width is reached. Even though no reconstruction is visible the atoms at the edges of the islands can move inwards slightly and thus reduce stress.

2. Magnetism: Wetting layer and 4th ML islands

We investigated the magnetic properties of a sample with 4th ML islands on top of the 2 ML wetting layer using spin-polarized STM. Figure 4 shows data acquired with a Fe-coated tungsten tip which is sensitive to the in-plane component of the sample magnetization. The topography (a) shows a sample of 3.0 ML Fe/W(001) [cf. Fig. 3(c)]. The corresponding dI/dU map in Fig. 4(b) is measured at a bias voltage of $U=-0.8$ V and shows a strong magnetic contrast for the 2nd ML which is presented in color scale (see also the full range of the color scale to the right in Fig. 4). For clarity the areas of the 3rd and 4th ML have been put to gray. One can distinguish four different contrasts on the 2nd ML denominated with small roman numbers $(i-iv)$ starting with the highest intensity. We have analyzed the strength of the different dI/dU signals of Fig. 4(b) (smoothed data) and found the following in arbitrary units (a.u.):

$$(dI/dU)_i = 2.26 \pm 0.08 \text{ a.u.},$$

$$(dI/dU)_{ii} = 1.92 \pm 0.08 \text{ a.u.},$$

$$(dI/dU)_{iii} = 1.74 \pm 0.09 \text{ a.u.},$$

$$(dI/dU)_{iv} = 1.40 \pm 0.13 \text{ a.u.}$$

Considering the fourfold symmetry of the (001) surface we can assume opposite magnetization for domains *i* and *iv* and for domains *ii* and *iii*, respectively. We calculated the amplitudes A of the dI/dU signal of oppositely magnetized domains,

$$A_{i-iv} = 0.86 \pm 0.15 \text{ a.u.},$$

$$A_{ii-iii} = 0.18 \pm 0.12 \text{ a.u.},$$

and on the basis of Eq. (1) we can calculate the relative orientation between tip magnetization $\vec{M}_t$ and sample magnetization $\vec{M}_s$,

$$\tan \alpha = \frac{A_{ii-iii}}{A_{i-iv}}. \tag{2}$$

α denominates the angle between $\vec{M}_t$ and $\vec{M}_s$, in this case the magnetization of domain *i*. We found

$$\alpha_{2\ \mathrm{ML}} = 11.8 \pm 7.9\ ^\circ .$$

This result is schematically drawn in Fig. 4(d) with $\vec{M}_t$ and $\vec{M}_s$ indicated by the arrows. The shaded regions mark the error. Although an opposite sense of rotation would also be consistent with our data, $\vec{M}_i$ is rotated arbitrarily anticlockwise by $\alpha_{2\ \mathrm{ML}}$. Figure 4(c) shows the same section of the surface at a different voltage measured simultaneously to (b) (forward and backward scan). At this voltage the 4th ML shows a strong magnetic contrast and is presented in color scale while the other layers are put to gray for better visibility. Again one can distinguish four different magnetic domains indicated with arabic numbers (1–4) from highest to lowest intensity. Comparing the domain structure of the 2nd ML [Figs. 4(b) and 4(d)] with that of the 4th ML no direct correlation is found. We analyzed the dI/dU signal of the 4th ML in the same way as described for the 2nd ML with

$$(dI/dU)_1 = 7.61 \pm 0.14 \text{ a.u.},$$

$$(dI/dU)_2 = 7.29 \pm 0.16 \text{ a.u.},$$

$$(dI/dU)_3 = 6.62 \pm 0.12 \text{ a.u.},$$

$$(dI/dU)_4 = 6.30 \pm 0.12 \text{ a.u.},$$

and calculated an angle of

$$\alpha_{4\ \mathrm{ML}} = 27.1 \pm 7.7^\circ$$

between the magnetization of the tip and the magnetization of domain 1 on the 4th ML as schematically sketched in Fig. 4(e). Here the arrow for $\vec{M}_1$ has been arbitrarily turned clockwise by $\alpha_{4\ \mathrm{ML}}$. Calculating the angle between 2nd and 4th ML magnetization for the two possible rotation directions of $\alpha_{2\ \mathrm{ML}}$ and $\alpha_{4\ \mathrm{ML}}$ ($\pm 11.8^\circ$ and $\pm 27.1^\circ$) one obtains angles of $15.3 \pm 11.0^\circ$ and $38.9 \pm 11.0^\circ$. Considering that we deal with a bcc (001) surface the only possible high-symmetry axes are $\langle 100 \rangle$ and $\langle 110 \rangle$. Therefore, the magnetization vectors of the 2nd and 4th ML must either be collinear or include an angle of 45°. Since a collinear arrangement is not within the error we conclude that a rotation of 45° is realized here.

To directly investigate the correlation between the magnetization of the 2nd ML with that of the 4th ML we closely compared the spatially resolved data of Figs. 4(b) and 4(c). We observe 4th ML islands with $\vec{M}_4$ both on patches with $\vec{M}_{iii}$ and $\vec{M}_{iv}$. Also 4th ML islands with $\vec{M}_3$ are present on two different domains of the 2nd ML, namely, $\vec{M}_{ii}$ and $\vec{M}_{iv}$. Islands with $\vec{M}_2$ are found on 2nd ML patches with $\vec{M}_i$ (not shown here) and $\vec{M}_{iii}$, while $\vec{M}_1$ is observed on $\vec{M}_i$ only. This indicates that the magnetization axes of the 4th ML lie in between the magnetization axes of the 2nd ML. We conclude that we observe a rotation of 45° between the magnetization axes of 2 ML and 4 ML as already proposed after analyzing the angles calculated from the dI/dU intensities. This result is sketched in Fig. 4(f).

Figure 5(a) shows a dI/dU map of again 3.0 ML Fe/W(001) with a spin-polarized tip at a larger scale and a sample bias of $U=-0.1$ V. Here the different magnetization axes of 2nd and 4th ML can be studied within the same image. We observe two different signal strengths of the 2nd ML denominated with *i* and *ii*. Three different contrasts (1–3) can be found for the 4th ML. There are no other contrasts not only on this section of the surface but on the whole area of the surface studied with this spin-polarized tip. Again we can assume four equivalent magnetization directions in each layer and can explain this measurement with an angle of $\approx 45^\circ$ between $\vec{M}_t$ and $\vec{M}_i$ and an angle of $\approx 0^\circ$ between $\vec{M}_t$ and $\vec{M}_1$ as sketched in Fig. 5(b). Again two types of 4th ML islands can be found on each of the 2 ML patches. This is

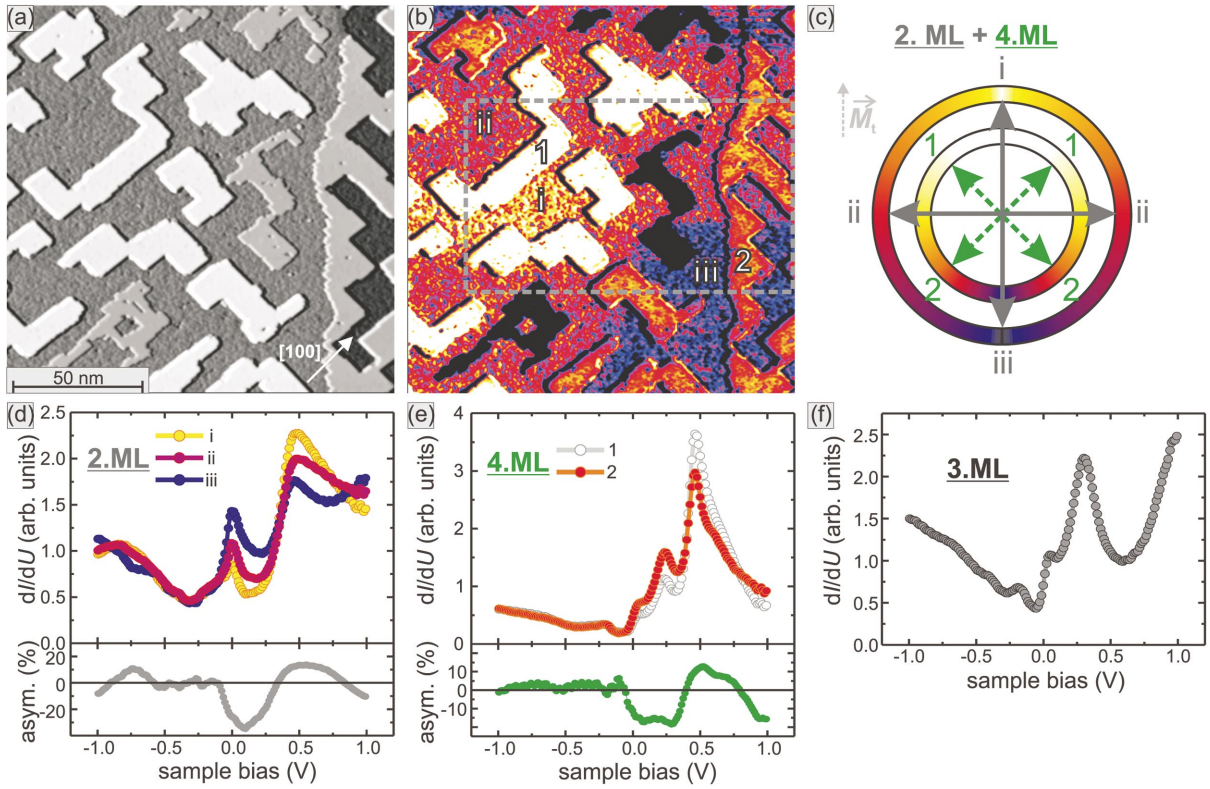

FIG. 6. (Color) Sample of 3.0 ML of Fe on W(001) grown at $T \approx 550$ K. (a) Topography at $U = +0.05$ V; (b) dI/dU map corresponding to (a) at $U = +0.05$ V; (c) sketch of the 45° rotation between 2nd and 4th ML magnetization; (d) dI/dU spectra of different magnetic domains (*i*, *ii*, *iii*) of the 2nd ML and asymmetry; (e) dI/dU spectra of different magnetic domains (1,2) of the 4th ML and asymmetry; (f) dI/dU spectra of the 3rd ML.

indicated in Fig. 5(a): islands with $\vec{M}_1$ and $\vec{M}_2$ on a patch with $\vec{M}_i$ and islands with $\vec{M}_2$ and $\vec{M}_3$ on a patch with $\vec{M}_{ii}$. We cannot differentiate between the two domains of the 4th ML which both have an angle of 90° to the $\vec{M}_t$, thus both are denominated with 2. Also the two domains of the 2nd ML with an angle of ±45° show the same strength of the dI/dU signal, the same holds for the two domains with $\alpha \approx \pm 135°$.

It is important to point out that a possible influence of the structure of the 4th ML islands on the magnetic properties has to be considered. As mentioned before the 4th ML islands are elongated due to a uniaxial inward relaxation at the island edges to partially relieve strain. Nevertheless it is observed that each island is magnetized homogeneously and no correlation of the magnetization direction with the long island axis is found. This leads to the conclusion that the effect of magnetoelastic coupling does not play a crucial role in this context.

Figures 6(a) and 6(b) show the topography and the corresponding dI/dU map of 3.0 ML Fe/W(001) at $U = +0.05$ V measured with a Fe-coated tip. In this case three different signal strengths of the 2nd ML (*i*–*iii*) but only two

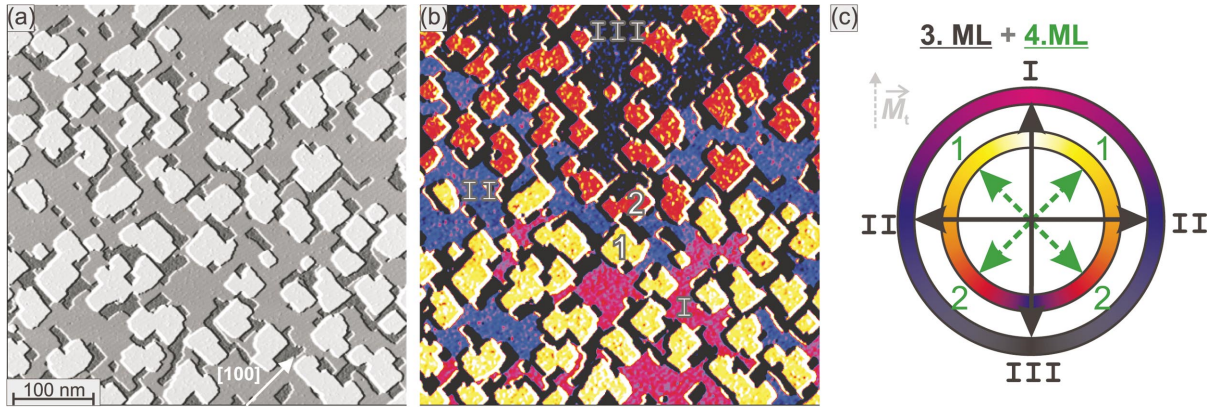

FIG. 7. (Color) Sample of 3.2 ML of Fe on W(001) grown at $T \approx 525$ K. (a) Topography at $U = +0.1$ V; (b) dI/dU map corresponding to (a) at $U = +0.1$ V; (c) sketch of the 45° rotation between 3rd and 4th ML magnetization.

nuances of the 4th ML (1,2) are detected in the dI/dU map (b). The explanation of these results is analog to the one for the previous measurements shown in Fig. 5 and the resulting magnetization axes with respect to $\vec{M}_t$ are shown in Fig. 6(c). Compared to Fig. 5(b) the magnetization of the tip used in this measurement is rotated by ≈45°. To investigate the spin polarization of the 2nd and 4th ML in more detail we performed spatially resolved full dI/dU spectroscopy (stabilization parameters: $U=+1.0$ V, $I=1$ nA) in the area indicated by the dashed rectangle in Fig. 6(b). The spin-resolved spectra for 2 and 4ML are shown in (d) and (e), a spectrum of the 3rd ML island in the image area is shown in (f). The spectra of the 2nd ML (d) show that $\vec{M}_{ii}$ is the intermediate of $\vec{M}_i$ and $\vec{M}_{iii}$. The two peaks observed for the 2nd ML are both highly spin polarized but with opposite sign. We observe an asymmetry of up to +14% for the peak at $U=+0.47$ V and up to −35% for the one at the Fermi energy $U=\pm 0.00$ V. Figure 6(e) shows three peaks for the 4th ML, the one at $U=+0.46$ V with an asymmetry up to +13%, the other ones have opposite spin polarization: $U=+0.24$ V with asymmetry −18%, $U=+0.03$ V with asymmetry −16%. The 3rd ML shows spectral features at $U=+0.30$ V, +0.05 V, and −0.18 V. In order to specify the character or cause of the different spectral features and to explain the different electronic structure of the pseudomorphic layers or the energy-dependent asymmetry, spin-resolved electronic structure calculations have to be performed for this system.

3. Magnetism: wetting layer, 3rd ML and 4th ML islands

To investigate the magnetic anisotropy of the 3rd ML we prepared a sample with growth conditions as described for Fig. 3(b). The topography and a corresponding dI/dU map at $U=+0.1$ V are shown in Figs. 7(a) and 7(b), respectively. The sample consists of a 2 ML thick wetting layer, connected patches of the 3rd ML and 4th ML islands. The dI/dU map at $U=+0.1$ V (b) shows magnetic contrast for both the 3rd and the 4th ML. Again we observe three contrast levels on one layer (3rd ML: I–III) and two on the other layer (4th ML: 1,2) and can conclude that the sample magnetization has an angle of ≈0° and ≈45° to $\vec{M}_t$, respectively. The derived magnetization axes for the 3rd and 4th ML are sketched in Fig. 7(c). Just as for the 2nd ML the magnetization of the 3rd ML also encloses an angle of 45° with that of the 4th ML. This leads to the conclusion that the 3rd ML couples collinearly to the layer underneath, while the layer on top, the 4th ML is magnetized along the other high-symmetry direction of the surface. The dI/dU signals of the small areas of uncovered 2nd ML also show magnetic contrast and a spatial correlation to the domains of the 3rd ML is found, while obviously no direct correlation is observed for the magnetization directions of 3rd and 4th ML. The collinear coupling between 2nd and 3rd ML was also observed in the measurement shown in Fig. 4: the 3rd ML islands indicated by the arrows in (a) also show a magnetic contrast in the dI/dU map at $U=-0.8$ V (b) which was hidden to avoid confusion when analyzing the 2nd ML regarding the magnetic signal. All 3rd ML islands on top of 2nd ML domains *i* show a particularly low dI/dU signal. 3rd ML islands on the oppositely magnetized domain *iv* appear very bright. A medium dI/dU signal is found for 3rd ML islands on top of domain *ii* while by chance there is no 3rd ML island on domain *iii* in the image area. Since an antiferromagnetic coupling between the 2nd and the 3rd ML is highly improbable we conclude that they couple ferromagnetically but possess an opposite spin polarization at this voltage. The measurement shown in Fig. 7 is a further confirmation that an influence of the uniaxial strain relief of the 4 ML islands of Figs. 4–6 on the direction of the magnetization can be excluded. Since a thermodynamical limit for the size of the 4th ML islands is found to be on the order of 10 nm the larger islands shown in Fig. 7 are considered to be fully strained except for a negligible fringe at the island edges. Therefore, it is concluded that the observed easy axis is an intrinsic property of the highly strained 4 ML thick areas and not a result of the strain relief.

4. Magnetism: Conclusions

The magnetic measurements show that the 2nd and 3rd ML couple magnetically collinear in moderately annealed samples of Fe on W(001) at a measurement temperature of $T\approx 13$ K. Even though there have been theoretical calculations that predict an antiferromagnetic monolayer,[28] an antiferromagnetic coupling between 2nd and 3rd ML is very unlikely and we conclude ferromagnetic coupling. With the method of SP-STM we are not able to determine the absolute direction of the magnetization and thus have to rely on measurements described in the literature. Since MOKE measurements[15,19] found an easy magnetization axis along ⟨110⟩ for the pseudomorphic growth regime of Fe on W(001) we conclude that the 2nd and 3rd ML both are magnetized along ⟨110⟩ or equivalent directions. We showed that the 4th ML has an easy axis which is rotated by 45° with respect to that of 2nd and 3rd ML. Thus the easy magnetization axis of the 4th ML is ⟨100⟩. This result is shown in Fig. 8.

It should be emphasized that in the samples studied the magnetization rotates from ⟨100⟩ to ⟨110⟩ and back on a scale of down to 10 nm. An estimate of the exchange length can be obtained by the evaluation of domain-wall widths. For the pseudomorphic layers investigated (2nd, 3rd, 4th ML) domain-wall widths on the order of 6 nm are observed (not shown here). The relation between the wall width w of 90° Néel walls, the exchange A and the magnetic anisotropy K is given by $w=4\sqrt{A/K}$. Taking the Fe bulk value $A=2\times 10^{-11}$ J/m and the measured domain-wall width one obtains a magnetic anisotropy of $\approx 2\times 10^6$ J/m^3, which is on the order of other values observed for thin iron films on

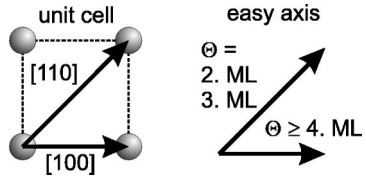

FIG. 8. Sketch of the unit cell of pseudomorphic Fe/W(001) together with the coverage dependent easy magnetization axes.

tungsten[29,30] (compared to the bulk value for Fe of $K \approx 5 \times 10^4$ J/m^3). The magnetization is considered to rotate on an even shorter length scale across the boundary between areas with different easy axes due to a reduced energy for a rotation of the magnetization by 45° only.

IV. SUMMARY AND OUTLOOK

In summary, we have presented a thorough investigation of the system of Fe on W(001) with an emphasis on the low coverage regime. We presented layer-resolved electronic structure measurements in terms of dI/dU spectra. Depending on local coverage very different features are found which cannot be explained on the basis of STM experiments. Theoretical calculations especially examining the pseudomorphic regime are desirable to gain further insight into the character of the spectral features. SP-STM measurements demonstrated that the sample of pseudomorphic Fe on W(001) with fourfold symmetry breaks up into several magnetic domains on the nanometer scale. The high spatial resolution as well as the magnetic sensitivity allows the investigation of up to eight different dI/dU signal strengths in one image and thus the direct correlation of magnetization directions of different layers with respect to the tip magnetization. The magnetic easy axes in the low coverage regime has been determined to rotate by 45° from ⟨110⟩ in layers with a local coverage of 2 and 3 ML to ⟨100⟩ at a local coverage of 4ML. We are convinced that further SP-STM measurements are useful to reach a more detailed understanding of the magnetic state of the monolayer of Fe on W(001) as well. Furthermore theoretical calculations are necessary to investigate the cause of the switching of the easy axis in the low coverage regime.

ACKNOWLEDGMENT

We acknowledge financial support from the DFG (Grant No. Wi1277/19-1 and Graduiertenkolleg "Design and characterization of functional materials").

*Electronic address: kbergman@physnet.uni-hamburg.de

[1] F. J. Himpsel, J. E. Ortega, G. J. Mankey, and R. F. Willis, Adv. Phys. **47**, 511 (1998).
[2] R. Allenspach, M. Stampanoni, and A. Bischof, Phys. Rev. Lett. **65**, 3344 (1990).
[3] R. Allenspach and A. Bischof, Phys. Rev. Lett. **69**, 3385 (1992).
[4] J. Thomassen, F. May, B. Feldmann, M. Wuttig, and H. Ibach, Phys. Rev. Lett. **69**, 3831 (1992).
[5] U. Gradmann, in *Handbook of Magnetic Materials*, edited by K. H. J. Buschow (Elsevier, Amsterdam, 1993).
[6] M. Speckmann, H. P. Oepen, and H. Ibach, Phys. Rev. Lett. **75**, 2035 (1995).
[7] J. Hauschild, U. Gradmann, and H. J. Elmers, Appl. Phys. Lett. **72**, 3211 (1998).
[8] S. Pütter, H. F. Ding, Y. T. Millev, H. P. Oepen, and J. Kirschner, Phys. Rev. B **64**, 092409 (2001).
[9] M. Bode, A. Kubetzka, O. Pietzsch, and R. Wiesendanger, Appl. Phys. A: Mater. Sci. Process. **72**, S149 (2001).
[10] A. Wachowiak, J. Wiebe, M. Bode, O. Pietzsch, M. Morgenstern, and R. Wiesendanger, Science **298**, 577 (2002).
[11] A. Yamasaki, W. Wulfhekel, R. Hertel, S. Suga, and J. Kirschner, Phys. Rev. Lett. **91**, 127201 (2003).
[12] X.-L. Zhou, C. Yoon, and J. M. White, Surf. Sci. **203**, 53 (1988).
[13] T. L. Jones and D. Venus, Surf. Sci. **302**, 126 (1994).
[14] H. J. Elmers and J. Hauschild, Surf. Sci. **320**, 134 (1994).
[15] W. Wulfhekel, F. Zavaliche, F. Porrati, H. P. Oepen, and J. Kirschner, Europhys. Lett. **49**, 651 (2000).
[16] W. Wulfhekel, F. Zavaliche, R. Hertel, S. Bodea, G. Steierl, G. Liu, J. Kirschner, and H. P. Oepen, Phys. Rev. B **68**, 144416 (2003).
[17] J. Chen, M. Drakaki, C. A. Ballentine, and J. L. Erskine, Bull. Am. Phys. Soc. **35**, 199 (1989).
[18] R. L. Fink, G. A. Mulhollan, A. B. Andrews, J. L. Erskine, and G. K. Walters, J. Appl. Phys. **69**, 4986 (1991).
[19] G. A. Mulhollan, R. L. Fink, J. L. Erskine, and G. K. Walters, Phys. Rev. B **43**, 13 645 (1991).
[20] J. Chen and J. L. Erskine, Phys. Rev. Lett. **68**, 1212 (1992).
[21] D. Venus and H. L. Johnston, Phys. Rev. B **50**, 15 787 (1994).
[22] M. Plihal, D. L. Mills, H. J. Elmers, and U. Gradmann, Phys. Rev. B **51**, 8193 (1995).
[23] R. Wu and A. J. Freeman, Phys. Rev. B **45**, 7532 (1992).
[24] R. Wiesendanger and M. Bode, Solid State Commun. **119**, 341 (2001).
[25] M. Bode, Rep. Prog. Phys. **66**, 523 (2003).
[26] O. Pietzsch, A. Kubetzka, D. Haude, M. Bode, and R. Wiesendanger, Rev. Sci. Instrum. **71**, 424 (2000).
[27] http://www.webelements.com
[28] R. Wu and A. J. Freeman, J. Magn. Magn. Mater. **127**, 327 (1993).
[29] M. Pratzer, H. J. Elmers, M. Bode, O. Pietzsch, A. Kubetzka, and R. Wiesendanger, Phys. Rev. Lett. **87**, 127201 (2001).
[30] A. Kubetzka, O. Pietzsch, M. Bode, and R. Wiesendanger, Phys. Rev. B **67**, 020401 (2003).